Image reconstruction from few views by ℓ_0-norm optimization

Sun Yu-Li(孙玉立) and Tao Jin-Xu(陶进绪)†

Department of Electronic Engineering and Information Science, University of Science and Technology of China, Hefei 230027, *China*

(Received 18 November 2013; revised manuscript received 17 January 2014; published online 15 May 2014)

In the medical computer tomography (CT) field, total variation (TV), which is the ℓ_1-norm of the discrete gradient transform (DGT), is widely used as regularization based on the compressive sensing (CS) theory. To overcome the TV model's disadvantageous tendency of uniformly penalizing the image gradient and over smoothing the low-contrast structures, an iterative algorithm based on the ℓ_0-norm optimization of the DGT is proposed. In order to rise to the challenges introduced by the ℓ_0-norm DGT, the algorithm uses a pseudo-inverse transform of DGT and adapts an iterative hard thresholding (IHT) algorithm, whose convergence and effective efficiency have been theoretically proven. The simulation demonstrates our conclusions and indicates that the algorithm proposed in this paper can obviously improve the reconstruction quality.

Keywords: iterative hard thresholding, few views reconstruction, sparse, ℓ_0-norm optimization

PACS: 87.57.Q–, 87.55.kd **DOI:** 10.1088/1674-1056/23/7/078703

1. Introduction

Image reconstruction from insufficient data is an important issue in computed tomography (CT). Insufficient data problems occur quite frequently because of practical constraints due to the imaging hardware, scanning geometry, or ionizing radiation exposure.[1] The insufficient data may arise from various forms, but in this work we only consider the few views reconstruction problem. Reconstruction by using standard analytic algorithms such as a filtered back-projection (FBP) algorithm will lead to distortion and artifact.

Mathematically, image reconstruction from a few views can be thought of as an underdetermined linear system. To overcome this ill-posed problem, we need to make some constraints to narrow the solution space. One type of them is based on the compressive sensing (CS) theory proposed by Candes *et al.*[2] The main idea of CS is that most signals are sparse in some appropriate representations; that is, a majority of their coefficients are close or equal to zero, when represented in these proper domains.[3] Then, CS reconstructs these sparse signals by using the ℓ_1-norm minimization.[3–7]

Because the X-ray attenuation coefficient often varies mildly within an anatomical component, and large changes are usually confined around the borders of tissue structures, discrete gradient transform (DGT) has been widely utilized as a sparsifying operator in CS-inspired CT reconstruction.[5–14] Without loss of generality, the corresponding ℓ_1-norm reconstruction problem can be described as

$$\min_{\boldsymbol{f}} \|\boldsymbol{f}\|_{\mathrm{TV}} = \min_{\boldsymbol{f}} \|\nabla \boldsymbol{f}\|_1, \ \text{s.t.}, \ \boldsymbol{R}\boldsymbol{f} = \boldsymbol{p}, \tag{1}$$

where $\boldsymbol{f}$ is the CT image to be reconstructed, $\boldsymbol{R}$ is the measurement matrix, $\boldsymbol{p}$ is the measured data, and $\|\boldsymbol{f}\|_{\mathrm{TV}}$ is the ℓ_1-norm of the DGT image $\nabla \boldsymbol{f}$, which is also referred to as the well-known total variation (TV) of $\boldsymbol{f}$. However, the DGT does not satisfy the restricted isometry property (RIP) required by the CS theory,[3] the ℓ_1-norm TV regularization is tending to uniformly penalize the image gradient and the low-contrast structures are sometimes over smoothed in the reconstruction.[14,15]

In this article, we focus on the ℓ_0-norm of the DGT image $\nabla \boldsymbol{f}$ and consider the following ℓ_0-norm minimization problem:

$$\boldsymbol{f}^* = \arg\min_{\boldsymbol{f}} \|\nabla \boldsymbol{f}\|_0, \ \text{s.t.}, \ \|\boldsymbol{R}\boldsymbol{f} - \boldsymbol{p}\|_2^2 \le e. \tag{2}$$

The optimization problem in Eq. (2) causes the image estimation with a minimum ℓ_0-norm constraint, such that the ℓ_2-distance between its projection data with the measured projection data is within a given tolerance e.

To the best of our knowledge, there are seldom reconstruction algorithms using the ℓ_0-norm of DGT. This is due to the fact that there are two main challenges in solving Eq. (2): first, the ℓ_0-norm minimization problem is known to be NP-hard; second, the DGT is not invertible in general, the Frobenius operator norm of its inverse grows linearly with the size of $\boldsymbol{f}$. In this work, we use the iterative hard thresholding (IHT) algorithm by Blumensath and Davies[16,17] to address the first challenge. We fix the sparsity level of the DGT image to an *a priori* known S, which means that the number of nonzero elements in $\nabla \boldsymbol{f}$ is less than S, and it can be obtained by FBP reconstruction of a similar image using full scan projections. We consider this optimization problem

$$\boldsymbol{f}^* = \arg\min_{\boldsymbol{f}} \|\boldsymbol{R}\boldsymbol{f} - \boldsymbol{p}\|_2^2, \ \text{s.t.}, \ \|\nabla \boldsymbol{f}\|_0 \le S. \tag{3}$$

†Corresponding author. E-mail: tjingx@ustc.edu.cn

© 2014 Chinese Physical Society and IOP Publishing Ltd

Inspired by the pseudo-inverse transform in the soft-threshold filtering by Yu and Wang,[7] we modify and apply it for this problem to address the second challenge. The numerical simulation shows that the proposed ℓ_0-norm algorithm can effectively improve the reconstruction quality.

The rest of the paper is structured as follows. In Section 2, we briefly review the IHT algorithm and propose the new ℓ_0-norm reconstruction algorithm. Section 3 presents the numerical results. In the end, we provide our conclusion in Section 4.

2. Method

2.1. IHT algorithm

Blumensath and his collaborator have proven the convergence of the IHT algorithm to solve the inverse problems regularized by a sparsity constraint.[16–20] Their major results can be summarized as follows.

A sparse or approximately sparse signal $\boldsymbol{f} = [f_1, f_2, \ldots, f_N] \in \mathbb{R}^N$ is sampled with a linear sampling operator $\boldsymbol{R} = (r_{m,n}) \in \mathbb{R}^{M\times N}$, $M \ll N$. The samples $\boldsymbol{p} \in \mathbb{R}^M$ are potentially corrupted by observation noise $\boldsymbol{e} \in \mathbb{R}^M$, that is

$$\boldsymbol{p} = \boldsymbol{R}\boldsymbol{f} + \boldsymbol{e}. \tag{4}$$

Under the assumption that we have known that $\boldsymbol{f}$ is K-sparse, then the reconstruction can be the following optimization problem:

$$\boldsymbol{f}^* = \arg\min_{\boldsymbol{f}} \|\boldsymbol{R}\boldsymbol{f} - \boldsymbol{p}\|_2^2 \ \text{ s.t., } \ \|\boldsymbol{f}\|_0 \le K. \tag{5}$$

Initialized with $\boldsymbol{f}^0 = \boldsymbol{0}$, the IHT algorithm uses the iteration[19–21]

$$\tilde{\boldsymbol{f}}^n = \boldsymbol{f}^{n-1} + \mu \boldsymbol{R}^{\mathrm{T}} \left(\boldsymbol{p} - \boldsymbol{R}\boldsymbol{f}^{n-1}\right), \tag{6}$$

$$\boldsymbol{f}^n = H_K\left(\tilde{\boldsymbol{f}}^n\right), \tag{7}$$

where μ is the step-size and $H_K\left(\tilde{\boldsymbol{f}}^n\right)$ is the non-linear operator that sets all but the K largest (in magnitude) elements in $\tilde{\boldsymbol{f}}^n$ to zero.[15]

From this, one can find that IHT is a very simple algorithm, it can be applied to image reconstruction[22] and it has been proved that IHT can recover near-optimal solutions of the sparse and approximately sparse signals under certain conditions.[17,19,23]

2.2. Algorithm development

In the CT reconstruction, a two-dimensional digital reconstructed image can be expressed as $\boldsymbol{f} = (f_{i,j}) \in \mathbb{R}^{I\times J}$, and to avoid ambiguity, we define

$$f_n = f_{i,j}, \ \ n = (i-1)\times J + j, \ \ N = I \times J, \tag{8}$$

to meet the model Eq. (5), and we will use both the signs f_n and $f_{i,j}$ next for convenience.

However, in the practical CT reconstruction, sparsity of images in terms of voxels $\boldsymbol{f}$ is generally not a widely applicable assumption, which means that model (5) cannot be used directly. As mentioned above, it is often the case that images have sparse DGT $\nabla\boldsymbol{f}$, then we change the model (5) as:

$$\boldsymbol{f}^* = \arg\min_{\boldsymbol{f}} \|\boldsymbol{R}\boldsymbol{f} - \boldsymbol{p}\|_2^2 \ \text{ s.t., } \ \|\nabla\boldsymbol{f}\|_0 \le S, \tag{9}$$

where $\|\nabla\boldsymbol{f}\|_0$ is the number of nonzero elements of $\nabla f_{i,j}$

$$\nabla f_{i,j} = \sqrt{\left(f_{i,j} - f_{i+1,j}\right)^2 + \left(f_{i,j} - f_{i,j+1}\right)^2}. \tag{10}$$

To solve the above optimization problem (9), we propose the projection onto convex sets (POCS) iterative hard thresholding (IHT-POCS) algorithm. The IHT-POCS has the following two main steps.

Step 1 Data projection iteration. In the typical IHT, a gradient descent step (6) is used to minimize the objective function; in the CT reconstruction here, we use the POCS to replace it. The reason is that even in the large-scale underdetermined system, POCS can still efficiently handle it and obtain a stable solution. We use the algebraic reconstruction technique (ART) algorithm instead of Eq. (6) to update the reconstruction: $\tilde{\boldsymbol{f}}^k = ART\left(\boldsymbol{f}^{k-1}\right)$, that is for $m = 1, 2, \ldots, M$

$$\begin{aligned} \tilde{\boldsymbol{f}}^{k,0} &= \boldsymbol{f}^{k-1}, \\ \tilde{\boldsymbol{f}}^{k,m} &= \tilde{\boldsymbol{f}}^{k,m-1} + \lambda^k \frac{p_m - \boldsymbol{R}_m \tilde{\boldsymbol{f}}^{k,m-1}}{\boldsymbol{R}_m \cdot \boldsymbol{R}_m^{\mathrm{T}}} \cdot \boldsymbol{R}_m^{\mathrm{T}}. \end{aligned} \tag{11}$$

Here, k is the main iteration number and $\boldsymbol{R}_m$ is the m-th row of measurement matrix $\boldsymbol{R}$. It should be noted that the ART used here can also be replaced by other POCS methods such as the simultaneous algebraic reconstruction technique (SART) and ordered-subset SART.

Step 2 IHT algorithm

$$\boldsymbol{f}^k = \nabla^{-1}(H_S(\nabla\tilde{\boldsymbol{f}}^k)). \tag{12}$$

As mentioned above, DGT of Eq. (10) is not invertible. Inspired by Yu and Wang's work in Ref. [7], we use ∇^{-1} as the pseudo-inverse transform of DGT.

Assume that w is the S-th largest element of $\nabla\tilde{\boldsymbol{f}}^k$, according to Eq. (12), when $\nabla\tilde{f}^k_{i,j} < w$, we should adjust the value of $\tilde{f}^k_{i,j}$, $\tilde{f}^k_{i+1,j}$, and $\tilde{f}^k_{i,j+1}$ to make $\nabla f^k_{i,j} = 0$; when $\nabla\tilde{f}^k_{i,j} \ge w$, we should keep the value of $\tilde{f}^k_{i,j}$, $\tilde{f}^k_{i+1,j}$, and $\tilde{f}^k_{i,j+1}$ unchanged to make $\nabla f^k_{i,j} = \nabla\tilde{f}^k_{i,j}$. This non-linear pseudo-inverse transform is

$$f^k_{i,j} = \frac{2f^{k,a}_{i,j} + f^{k,b}_{i,j} + f^{k,c}_{i,j}}{4}, \tag{13}$$

$$f^{k,a}_{i,j} = \begin{cases} \dfrac{\tilde{f}^k_{i,j} + \tilde{f}^k_{i+1,j} + \tilde{f}^k_{i,j+1}}{3}, & \nabla\tilde{f}^k_{i,j} < w, \\ \tilde{f}^k_{i,j}, & \nabla\tilde{f}^k_{i,j} \ge w, \end{cases} \tag{14}$$

$$f^{k,b}_{i,j} = \begin{cases} \dfrac{\tilde{f}^k_{i-1,j} + \tilde{f}^k_{i,j} + \tilde{f}^k_{i-1,j+1}}{3}, & \nabla\tilde{f}^k_{i-1,j} < w, \\ \tilde{f}^k_{i,j}, & \nabla\tilde{f}^k_{i-1,j} \ge w, \end{cases} \tag{15}$$

$$f_{i,j}^{k,c} = \begin{cases} \dfrac{\tilde{f}_{i,j-1}^{k} + \tilde{f}_{i,j}^{k} + \tilde{f}_{i+1,j-1}^{k}}{3}, & \nabla \tilde{f}_{i,j-1}^{k} < w, \\ \tilde{f}_{i,j}^{k}, & \nabla \tilde{f}_{i,j-1}^{k} \geq w. \end{cases} \quad (16)$$

The flow chart of IHT-POCS is shown in Table 1, where N_{iter} is the max number of reconstruction iterations; λ is the relaxation parameter that can be set to constant 1 or other values, for example, $\lambda = 1.0 \times 0.99^k$; the positivity constraint can be freely chosen; ε^k is the ℓ_2-distance between two iterative images $\boldsymbol{f}^k$ and $\boldsymbol{f}^{k-1}$. When $\varepsilon^k < \varepsilon_0$, this exit criterion means that there is no longer any appreciative changes in the iteration and the IHT-POCS algorithm runs into convergence.

Table 1. Implementation steps of IHT-POCS reconstruction.

Algorithm of IHT-POCS
Initialization
Given $\boldsymbol{R}$, $\boldsymbol{p}$, N_{iter}, λ, S, and ε_0
$\boldsymbol{f}^0 = \boldsymbol{0}$
Main iteration loop
for $k = 1, 2, 3, \ldots, N_{\text{iter}}$ do
ART updating
$\tilde{\boldsymbol{f}}^{k,0} = \boldsymbol{f}^{k-1}$
for $m = 1, 2, 3, \ldots, M$ do
$\tilde{\boldsymbol{f}}^{k,m} = \tilde{\boldsymbol{f}}^{k,m-1} + \lambda^k \dfrac{p_m - \boldsymbol{R}_m \tilde{\boldsymbol{f}}^{k,m-1}}{\boldsymbol{R}_m \cdot \boldsymbol{R}_m^{\mathrm{T}}} \cdot \boldsymbol{R}_m^{\mathrm{T}}$
end
Positivity constraint
$\tilde{f}_{i,j}^{k} = \begin{cases} \tilde{f}_{i,j}^{k,M}, & \tilde{f}_{i,j}^{k,M} \geq 0 \\ 0, & \tilde{f}_{i,j}^{k,M} < 0 \end{cases}$
Iterative hard thresholding
Calculate $\nabla \tilde{\boldsymbol{f}}^k$, w
Perform the non-linear filter $\boldsymbol{f}^k = \nabla^{-1}\left(H_{\text{S}}\left(\nabla \tilde{\boldsymbol{f}}^k\right)\right)$
by using Eqs. (13) (14) (15), and (16)
Exit criterion
$\varepsilon^k = \left\| \boldsymbol{f}^k - \boldsymbol{f}^{k-1} \right\|_2$
if $\varepsilon^k < \varepsilon_0$ then
exit
end
end

3. Simulation

In this section, simulation is performed to demonstrate the proposed conclusions and evaluate the performance of the IHT-POCS algorithm. We apply four methods to reconstruct the images: 1) the classical ART method without using any sparsity regularizations; 2) the ART iteration with TV regularization method (ART-TV) as in Ref. [1]; 3) the iterative soft thresholding with TV regularization method (IST-TV) as in Ref. [7]; 4) the proposed IHT-POCS method using the ℓ_0-norm of the DGT image. For all the above methods, the parameter λ^k in the ART iteration in Eq. (11) is set to be constant 1.

In the first study, we assume that the sparsity level S of the reconstructed image is known, this can be obtained by FBP reconstruction of a similar image using full scan projections. Firstly, we use the well-known 128×128 modified Shepp–Logan phantom and set $S = 1081$. Figure 1 shows the few views image reconstructions based on different methods from 21 projections after 800 iterations; Figure 2 shows the IHT-POCS reconstructions after different numbers of iterations. It should be noted that the performance of ART-TV is not as good as expected here, this may be partly because the parameters we selected in ART-TV failed to balance TV-gradient descent with data constraints. After trying different choices of parameters, we pick out the one that provides the best performance. Comparing Fig. 1(d) with other reconstructed images, one can find that the proposed IHT-POCS algorithm can overcome the TV model's disadvantageous tendency of over smoothing the low-contrast structures, and it can also improve the quality of reconstruction.

Here we also use three evaluation parameters to evaluate the reconstructed image: the normalized mean square distance (d), the normalized absolute average distance (r),[24] and the peak signal to noise ratio (PSNR).

$$d = \left(\frac{\sum_{i=1}^{N}\sum_{j=1}^{N} (t_{i,j} - f_{i,j})^2}{\sum_{i=1}^{N}\sum_{j=1}^{N} (t_{i,j} - \bar{t})^2} \right)^{1/2}, \quad r = \frac{\sum_{i=1}^{N}\sum_{j=1}^{N} |t_{i,j} - f_{i,j}|}{\sum_{i=1}^{N}\sum_{j=1}^{N} |t_{i,j}|}, \quad (17)$$

where t is the test standard image, $\bar{t}$ is the average value of t, and f is the reconstructed image. One can see that d is sensitive to big errors, while r is sensitive to whole errors.

Figure 3 shows the evaluation parameters of the reconstructions based on ART-TV, IST-TV, and IHT-POCS from 21 projections on each iteration. From this, one can find that the IHT-POCS algorithm can gain a much faster convergence and better reconstruction quality than the other algorithms.



Fig. 1. Reconstructed images of a modified Shepp–Logan phantom from 21 projections after 800 iterations. Panels (a)–(d) correspond to the reconstructions using ART only, ART-TV, IST-TV, and IHT-POCS, respectively. The last panel (e) is the original phantom. The display window is [0.1, 0.35].



Fig. 2. The reconstructions based on IHT-POCS from 21 projections after different numbers of iterations. Panels (a)–(d), corresponding to the numbers of iterations which are 100, 200, 400, and 800, respectively. The last panel (e) is the ideal phantom. The display window is [0.15, 0.25].

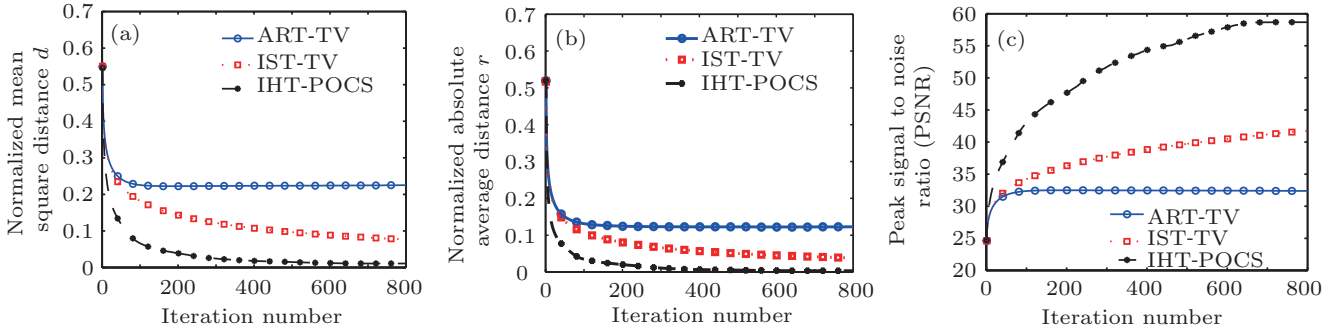


Fig. 3. (color online) The evaluation parameters of the reconstructions based on ART-TV, IST-TV, IHT-POCS: d (a), r (b), and PSNR (c).

Secondly, to challenge the proposed algorithm, we also repeat the above experiment in the 256×256 2D FORBILD head phantom.[25] Figure 4 shows the few views image reconstruction from 41 projections after 800 iterations. A similar simulation without IHT-POCS can be found in Fig. 6 in Ref. [7], although it uses the SART instead of ART. Table 2 lists the evaluation parameters for comparing these algorithms under different phantoms. This result once again indicates that the proposed IHT-POCS can gain a better reconstruction.

Table 2. Performance comparison of different algorithms under different phantoms.

Phantom	Parameters	ART	ART-TV	IST-TV	IHT-POCS
Shepp–Logan phantom	d	0.5376	0.2250	0.0763	0.0109
	r	0.5934	0.1227	0.0381	0.0033
	PSNR	24.8223	32.3865	41.7783	58.6828
FORBILD head phantom	d	0.2580	0.1369	0.0697	0.0048
	r	0.1518	0.0347	0.0152	0.0007
	PSNR	15.9103	21.4144	27.2755	50.4422

In the second study, the sparsity level S of the reconstructed image is unknown. From Eq. (9), we can see that the data residual $\sigma(S) = \|\boldsymbol{p} - R\boldsymbol{f}\|_2^2$ is dependent on S. When S is equal to N, then $\sigma(S)$ is close to 0. The overall trend is that $\sigma(S)$ varies inversely as S, but when S is very close to the actual sparsity, $\sigma(S)$ reaches a local minimum; once S is smaller than the actual sparsity, then $\sigma(S)$ will increase suddenly. From the data error $\sigma(S)$–sparsity S chart, one can estimate the DGT image sparsity level. This is illustrated in Fig. 5, where there is a sudden change at $S = 2^{11}$, which means that the real sparsity is between 2^{11} and 2^{10}; then we can use the dichotomy searching method to make its scope further narrowed, and our several experiments indicate that it would be better that the estimation is loose and a little greater than the actual value. Here, the actual sparsity $S_* = 1081$ and $\sigma(S_*) = 0.4227$. It should be noted that due to the actual sparsity S_* is close to 2^{10}, it is nature that the largest change in this rough chart is between 2^{10} and 2^9. If the sparsity level is unknown, we can estimate it first and then reconstruct the image by using the IHT-POCS algorithm based on the estimated S.

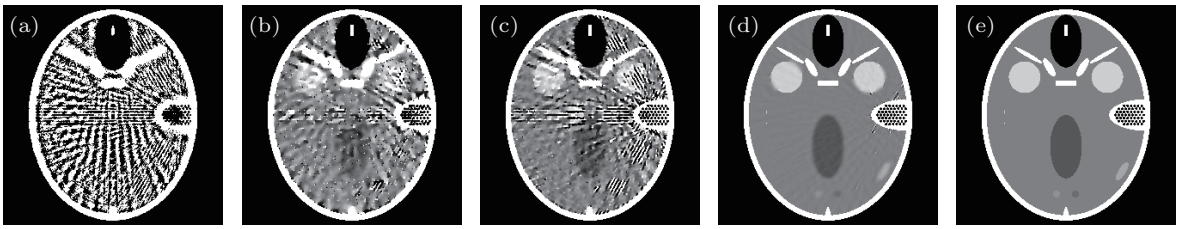


Fig. 4. Reconstructed images of FORBILD head phantom from 41 projections after 800 iterations. Panels (a)–(d) correspond to the reconstructions using ART only, ART-TV, IST-TV, and IHT-POCS, respectively. The last panel (e) is the original phantom. The display window is [1.035, 1.065].

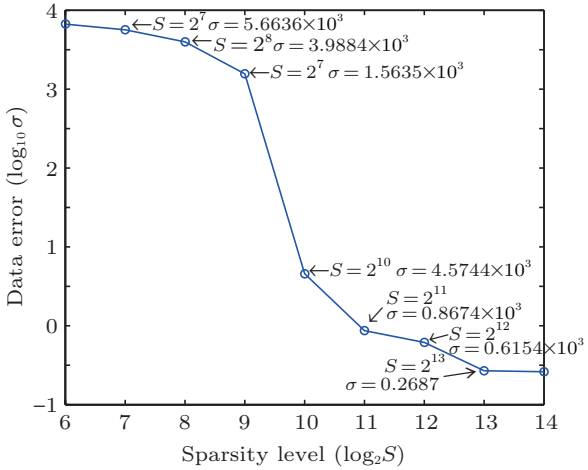


Fig. 5. (color online) Data errors at different sparsity level estimations, under the same conditions as those in Fig. 1.

4. Conclusion

In this paper, we propose a new iterative algorithm to reconstruct the image from a few views, which uses the ℓ_0-norm of the DGT as the regularization. The proposed algorithm uses a pseudo-inverse transform of DGT and adapts the IHT algorithm to address the challenges introduced by the ℓ_0-norm DGT. The simulation shows that this algorithm can effectively improve the reconstruction quality. Meanwhile, as shown in the simulation, the sparse level can only be roughly estimated, so how to obtain the accurate estimation is still unresolved for us, which is also our next work. In the near future, we will evaluate the algorithm with physical as well as clinical datasets, and investigate other reconstruction methods to deal with the ℓ_0-norm optimization. As the few views reconstruction has varied application demands in many fields, we believe that the proposed reconstruction algorithm is expected to have potential practical merits.

References

[1] Sidky E Y, Kao C M and Pan X C 2006 *J. X-Ray Sci. Technol.* **14** 119
[2] Candes E J, Romberg J and Tao T 2006 *IEEE Trans. Inform. Theory* **52** 489
[3] Yu H Y and Wang G 2010 *J. Biomed. Imaging* **2010** 934847
[4] Wang L Y, Li L, Yan B, Jiang C S, Wang H Y and Bao S L 2010 *Chin. Phys. B* **19** 088106
[5] Li S P, Wang L Y, Yan B, Li L and Liu Y J 2012 *Chin. Phys. B* **21** 108703
[6] Zhang H M, Wang L Y, Yan B, Li L, Xi X Q and Lu L Z 2013 *Chin. Phys. B* **22** 078701
[7] Yu H Y and Wang G 2010 *Phys. Med. Biol.* **55** 3905
[8] Velikina J, Leng S and Chen G H 2007 *Medical Imaging* 2007*: Physics of Medical Imaging*, February 17, 2007, San Diego, CA, p. 651020
[9] Sidky E Y and Pan X C 2008 *Phys. Med. Biol.* **53** 4777
[10] LaRoque S J, Sidky E Y and Pan X C 2008 *J. Opt. Soc. Am. A* **25** 1772
[11] Han X, Bian J G, Ritman E L, Sidky E Y and Pan X C 2012 *Phys. Med. Biol.* **57** 5245
[12] Duan X H, Zhang L, Xing Y X, Chen Z Q and Cheng J P 2009 *IEEE Trans. Nucl. Sci.* **56** 1377
[13] Chen Z Q, Jin X, Li L and Wang G 2013 *Phys. Med. Biol.* **58** 2119
[14] Feng J and Zhang J Z 2013 *Int. J. Imag. Syst. Tech.* **23** 44
[15] Herman G T and Davidi R 2008 *Inverse Probl.* **24** 045011
[16] Blumensath T and Davies M E 2008 *J. Fourier Anal. Appl.* **14** 629
[17] Blumensath T and Davies M E 2009 *Appl. Comput. Harmon. A* **27** 265
[18] Blumensath T and Davies M E 2009 *IEEE International Conference on Acoustics, Speech and Signal Processing*, April 19–24, 2009, Taipei, p. 3357
[19] Blumensath T and Davies M E 2010 *IEEE J. Select. Topics in Signal Process.* **4** 298
[20] Blumensath T 2012 *Signal Process.* **92** 752
[21] Cevher V 2011 *Proceedings of SPIE* 8138 *Wavelets and Sparsity XIV*, September 27, 2011, San Diego, USA, p. 813811
[22] Sidky E Y, Anastasio M A and Pan X C 2010 *Opt. Express* **18** 10404
[23] Maleki A 2009 47*th Annual Allerton Conference on Communication, Control, and Computing*, September 30, 2009, Monticello, USA, p. 236
[24] Zhuang T G 1992 *Computed Tomography Theory and Algorithm* (Shanghai: Shanghai Jiaotong University Press) p. 11 (in Chinese)
[25] Yu Z C, Noo F, Dennerlein F, Wunderlich A, Lauritsch G and Hornegger J 2012 *Phys. Med. Biol.* **57** N237